Article

JOURNAL OF THE CHINESE CHEMICAL SOCIETY

Experimental and Theoretical Studies of 4-(1-benzyl-5-methyl-1*H*-1,2,3-triazol-4-yl)-6-(2,4-dichlorophenyl)pyrimidin-2-amine: A Potential Antibacterial Agent

S. Murugavel,[a]* R. Madhanraj,[b] D. K. Andrew Prasanna Kumar,[a] Sangaraiah Nagarajan[c] and Alagusundaram Ponnuswamy[c]

[a]*Department of Physics, Thanthai Periyar Government Institute of Technology, Vellore-632 002, Tamilnadu, India*
[b]*Department of Physics, Ganadipathy Tulsi's Jain Engineering College, Kaniyambadi, Vellore-632102*
[c]*Department of Organic Chemistry, School of Chemistry, Madurai Kamaraj University, Madurai-625021, Tamilnadu*

(Received: Jan. 8, 2015; Accepted: May 27, 2015; Published Online: Jul. 8, 2015; DOI: 10.1002/jccs.201500010)

The title compound (**1**), 4-(1-benzyl-5-methyl-1*H*-1,2,3-triazol-4-yl)-6-(2,4-dichlorophenyl)pyrimidin-2-amine ($C_{20}H_{16}Cl_2N_6$), was synthesized and structurally characterized by elemental analysis, ^{1}H NMR and ^{13}C NMR and single crystal X-ray diffraction. The compound crystallizes as a colourless needle shaped in the triclinic system, space group P-1 with cell constants: a = 10.7557(11) Å, b = 12.7078(17) Å, c = 15.511(2) Å, α = 68.029(4)°, β = 86.637(5)°, γ = 87.869(4)°; V = 1962.4 (4) Å^3, Z = 4. There are two structurally similar but crystallographically independent molecules (A and B) in the asymmetric unit of the title compound, which is linked *via* N-H…Cl hydrogen bond. An intramolecular C-H…N hydrogen also occurs in each molecule. In the crystal, each of independent molecules forms a centrosymmetric dimer with an $R^2_2(8)$ ring motifs through a pair of N-H…N hydrogen bonds. These dimers are further connected by intermolecular N-H…Cl and C-H…Cl hydrogen bonds, forming an infinite two dimensional supramolecular network lying parallel to the [010] plane. The molecular geometry was also optimized using density functional theory (DFT/B3LYP) method with the 6-311G (d, p) basis set and compared with the experimental data. Mulliken population analyses on atomic charges, HOMO-LUMO energy levels, Molecular electrostatic potential and chemical reactivity of the title compound were investigated by theoretical calculations. The thermo dynamical properties of the title compound at different temperature have been calculated and corresponding relations between the properties and temperature have also been obtained. The *in vitro* antibacterial activity has been screened against Gram-positive (*Bacillus cerus* and *Staphylococcus epidermidis*) and Gram-Negative (*Escherichia coli*, *Acinetobacter baumannii* and *Proteus vulgaris*). The results revealed that the compound exhibited good to moderate antibacterial activity.

Keywords: X-ray structure determination; Hydrogen bonds; DFT calculations; HOMO-LUMO; MEP; Chemical reactivity; Antibacterial activity.

INTRODUCTION

1,2,3-triazoles have been found a wide range of important applications in the pharmaceutical, polymer, and material fields.[1] In addition, they have shown a broad spectrum of biological properties such as anti-bacterial,[2] anti-allergic,[3] anti-HIV activity[4] and also serve as potential chemotherapeutic agents for various diseases.[5] On the other hand, substituted pyrimidine nuclei were found anti-viral,[6] anti-tubercular, antineoplastic, anti-inflammatory, diuretic, antimalarial and cardiovascular.[7] In view of these bioactivities of the individual heterocycles, it was envisaged that the synthesis of novel hybrid molecules containing two of the above said moieties in a single frame is worth to attempt. Literature survey reveals that so for there is no experimental and theoretical studies for the title compound. In recent years, density functional theory (DFT) has become an increasingly useful tool for theoretical studies. It is also computationally less demanding than wave function based methods with inclusion of electron correlation.[8,9] Thus, in order to characterize the correlation between molecular structure and macroscopic properties in the studied compound, it seems to be essential to undertake a detailed comparative study of the isolated molecule and the solid state unit. In this paper, we report the synthesis, crystal structure and antibacterial activity of 4-(1-benzyl-5-methyl-1*H*-1,2,3-triazol-4-yl)-6-(2,4-dichlorophenyl) pyrimidin-2-amine ($C_{20}H_{16}Cl_2N_6$), as well as theoretical studies using the DFT(B3LYP) method and 6-311G(d, p) basis set. The aim of the present work was to describe and characterize the molecular structure and some electronic

* Corresponding author. Tel: +919790084145; Email: smurugavel27@gmail.com

Supporting information for this article is available on the www under http://dx.doi.org/10.1002/jccs.201500010

structure properties of the title compound, both experimentally and theoretically. We also make comparisons between experimental and calculated values. The *in vitro* antibacterial activity has been screened against Gram-positive (*Bacillus cerus* and *Staphylococcus epidermidis*) and Gram-Negative (*Escherichia coli*, *Acinetobacter baumannii* and *Proteus vulgaris*) at three different concentrations 25, 50 and 75 μg/ml. The results were evaluated by measuring the inhibition zones diameter in millimeters and were compared with the standard antibiotic ciprofloxacin (25 μg/ml)

RESULTS AND DISCUSSION

Description of Crystal structure

The displacement ellipsoid plot and theoretical geometry structure with the atom-numbering scheme for compound (**1**) is shown in Fig. 1. The compound (**1**) crystallizes as a colourless needle shaped in the triclinic system, space group P-1 with cell constants: a = 10.7557(11) Å, b = 12.7078(17) Å, c = 15.511(2) Å, α = 68.029(4)°, β = 86.637(5)°, γ = 87.869(4)°; V = 1962.4 (4) Å^3, Z = 4. Details of the data collection, crystal parameters and refinement process of compound (**1**) are given in Table 1.

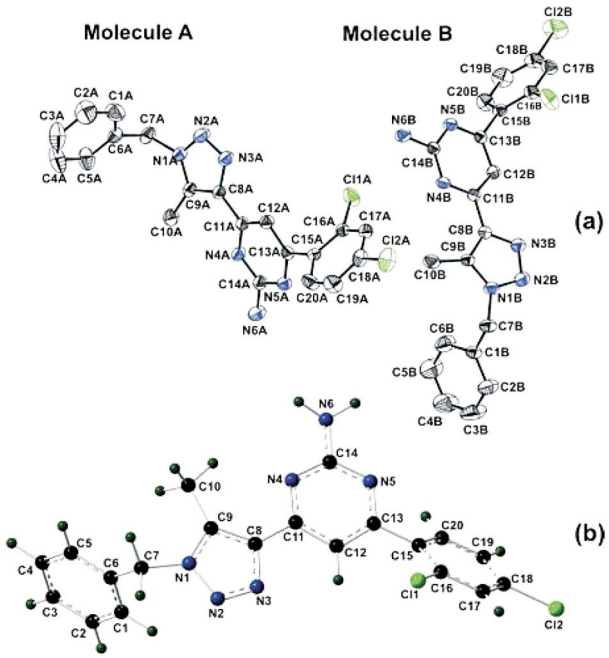

Fig. 1. **(a)** View of title compound showing two crystallographically independent molecules (A and B) with the atom-numbering scheme. Displacement ellipsoids for the non-H atoms are drawn at the 30% probability level. The H atoms are presented with spheres with arbitrary radii. **(b)** The theoretical geometric structure of the title compound (B3LYP/6-311G(d,p) level).

The asymmetric unit of the title compound contains two crystallographically independent molecules (A and B). The triazole ring(N1A-N4A/C8A/C9A and N1B-N4B/C8B/C9B) of both molecules A and B are essentially planar [maximum deviation -0.004(3) Å for C8A molecule A and 0.005(3) Å for C9B in molecule B] and they form dihedral angle of 11.8 (2)° and 8.1 (1)°, respectively, with essentially planar pyrimidine ring [maximum deviation C13A 0.004(3) for C13A and 0.003(3) for C14B] as both molecule A and B. The dihedral angle between two benzene rings is 64.7 (2)° and 65.7 (2)° in molecules A and B, respectively. The benzene ring attached to pyrimidine ring is in bisection position in molecule A and equatorial position

Table 1. Crystal and experimental data for the compound (**1**)

Empirical formula	$C_{20}H_{16}Cl_2N_6$
Formula weight	411.29
Temperature (K)	293(2)
Wavelength (Å)	0.71073
Crystal system	Triclinic
Space group	P $\bar{1}$
Unit cell dimensions(Å, °)	
a	10.7557(11)
b	12.7078(17)
c	15.511(2)
α	68.029(4)
β	86.637(5)
γ	87.869(4)
Volume (Å^3)	1962.4(4)
Z	4
Calculated density (Mg/m^3)	1.392
Absorption coefficient (mm^{-1})	0.349
F(000)	848
Crystal size (mm^3)	0.30 × 0.24 × 0.11
Theta range for data collection (°)	1.90 to 28.36
Index ranges	-14 <= h <= 13,
	-13 <= k <= 16,
	-10 <= l <= 20
Reflections collected	11403
Independent reflections	9200 [R(int) = 0.0184]
Completeness to theta = 28.34°	98.0 %
Refinement method	Full-matrix least-squares on F^2
Data/restraints/parameters	9200/1/507
Goodness-of-fit on F^2	1.019
Final R indices [I > 2σ(I)]	R1 = 0.0565, wR2 = 0.1324
R indices (all data)	R1 = 0.1205, wR2 = 0.1632
Largest diff. peak and hole (e.Å^{-3})	0.388 and -0.289

in molecule B. The bond distances for molecule A is N3–C8, C8–C9, C9–N1, N1–N2 and N2–N3 are 1.368(4), 1.368(4), 1.345(3), 1.345(4) and 1.305 (3) Å, respectively, which agrees with C=C, N=N, C–N distances found in literature for compound having triazole heterocycles.[10,11] In pyrimidine ring the N–C bond lengths [1.339(2)–1.357(2) Å] and bond angles N6–C14–N5 [117.0(2)°] are found close to the reported values for similar pyrimidine derivatives.[12]

The two independent molecules A and B are linked *via* N6B–H1NB...Cl1A hydrogen bonds. Also, the molecular conformation is stabilized by intramolecular C10A–H10B...N4A and C10B–H10A...N4B hydrogen bonds in molecule A and molecule B, respectively, both forming S(6) ring motifs. In the crystal packing, each inversion-related molecules of A and B form a centrosymmetric dimer through intermolecular N6A–H2NA...N5A and N6B–H2NB...N5B hydrogen bonds, respectively, each locally creates a $R_2^2(8)$ ring motifs. This dimers are further connected by intermolecular N6A–H1NA...Cl1B and C19A–H19A...Cl2B hydrogen bonds forming an infinite two dimensional supramolecular network lying parallel to the [0 1 0] plane [Table 2 and Fig. 2]

DFT calculations

The first task of the computational work is to determine the optimized geometry of the title compound. The starting coordinates were obtained from X-ray structure determination. The optimized parameters (bond lengths, bond angles) of the compound (**1**) were obtained using (DFT/B3LYP) method with the 6-311G(d,p) basis set. The results are listed in Table 3 and compared with the experimental data for the title compound.

As seen from the Table 3, the agreement between the theoretically calculated and the experimentally obtained structure parameters for the title compound are very good.

Table 2. Hydrogen bonding geometry for compound (**1**) (Å, °)

D–H...A	d(D–H)	d(H...A)	d(D...A)	< (DHA)
N6B–H1NB...CL1A	0.86	2.55	3.398(3)	169.0
C10A–H10B...N4A	0.96	2.47	3.082(4)	121.0
C10B–H10E...N4B	0.96	2.46	3.093(2)	123.0
N6A–H2NA...N5A [i]	0.86	2.23	3.033(3)	154.5
N6B–H2NB...N5B [ii]	0.86	2.22	3.011(3)	153.8
N6A–H1NA...Cl1B [iii]	0.86	2.57	3.423(3)	169.8
C19A–H19A...Cl2B [iv]	0.93	2.67	3.602(3)	176.4

Symmetry codes (i) -x + 1, -y + 1, -z; (ii) -x + 2, -y + 1, -z + 1; (iii) x, y, z - 1; (iv) x - 1, y + 1, z - 1.

In view of the bond lengths in Table 3, most predicted values are longer than experimental ones. We note that the experimental results are for the solid phase and the theoretical calculations are for the gas phase. In the solid state, the existence of a crystal field along with the intermolecular interactions connect the molecules together, which results in the difference in bond parameters between the calculated and experimental values.[13]

When the X-ray structure of the title compound was compared with its optimized counterpart (see Fig. 1), conformational discrepancies were observed. The orientation of the phenyl rings of compound (**1**) proved the most notable discrepancy, and is defined with torsion angle N5–C13–C15–C20 = -54.6° (Molecule A) and -75.7° (Molecule B) and C5–C6–C7–N1 = 102.4° (Molecule A) and -42.6° (Molecule B), which is calculated at -40.1° and -131.9°, respectively, for B3LYP/6-311G(d,p) level.

A global comparison was performed by superimposing the molecular skeletons obtained from X-ray diffraction and the theoretical calculations atom by atom (see Fig. 3), obtaining RMSE's values of 0.544, 0.540 and 0.766 Å by superimposing molecule A with molecule B, molecule A with optimized structure and molecule B with optimized structure, respectively. This magnitude of RMSE can be explained by the fact that the intermolecular columbic interaction with the neighboring molecules are absent in gas phase, whereas the experimental result corresponds to interacting molecules in the crystal lattice.

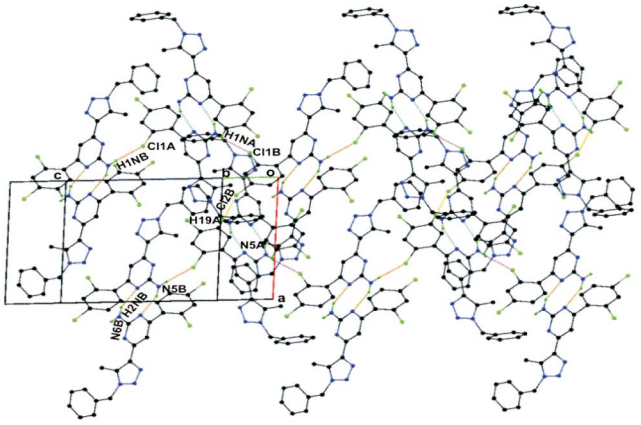

Fig. 2. View of two dimensional supramolecular network parallel to [0 1 0] plane showing N–H…N (brown and cyan lines), N–H…Cl (purple lines) and C–H…Cl (yellow lines) interactions. Hydrogen atoms not included in the hydrogen bonding are omitted for clarity.

Table 3. Selected structural parameters by X-ray diffraction and DFT calculations for compound (**1**)

Parameters	X-ray		DFT
	Molecule A	Molecule B	
Bond lengths (Å)			
C12-C13	1.381(4)	1.373(4)	1.392
C13-N5	1.335(3)	1.331(3)	1.341
C14-N4	1.343(3)	1.335(3)	1.342
C14-N5	1.343(3)	1.351(3)	1.340
C14-N6	1.348(4)	1.347(3)	1.368
C15-C16	1.373(4)	1.375(4)	1.402
C16-C17	1.385(4)	1.375(4)	1.393
C16-Cl1	1.736(3)	1.727(3)	1.759
C17-C18	1.365(4)	1.358(4)	1.387
C18-C19	1.364(5)	1.369(5)	1.390
C18-Cl2	1.732(3)	1.733(3)	1.756
C19-C20	1.374(4)	1.379(4)	1.387
Bond angles (°)			
N5-C13-C12	122.6(2)	122.2(2)	121.80
N4-C14-N5	126.1(3)	126.2(2)	126.54
N4-C14-N6	117.0(3)	117.5(2)	116.91
N5-C14-N6	117.0(2)	116.4(2)	116.53
C15-C16-C17	123.1(2)	123.2(3)	121.70
C15-C16-Cl1	119.7(2)	119.3(2)	122.06
C17-C16-Cl1	117.1(2)	117.4(2)	119.15
C18-C17-C16	117.7(3)	117.7(3)	119.15
C19-C18-C17	121.5(3)	121.6(3)	121.10
C19-C18-Cl2	118.9(2)	119.2(3)	119.75
C17-C18-Cl2	119.6(3)	119.1(3)	119.15
C18-C19-C20	119.2(3)	119.6(3)	118.63
C19-C20-C15	121.9(3)	120.7(3)	122.43
C13-N5-C14	116.2(2)	116.1(2)	116.53
Torsion angles (°)			
N5-C13-C15-C20	-54.6(4)	-75.7(4)	-40.1
C5–C6–C7–N1	- 102.4(4)	-42.6(1)	-131.9
C15-C13-N5-C14	178.7(2)	-179.1(2)	177.6
N6-C14-N4-C11	-179.4(1)	-179.0(3)	177.5

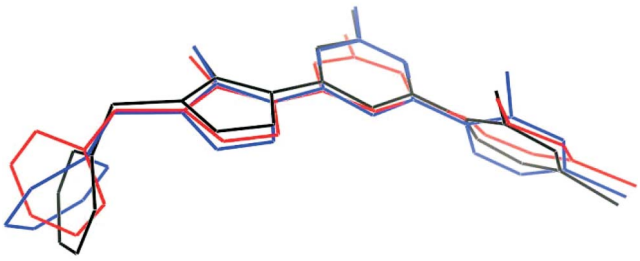

Fig. 3. Atom-by-atom superimposition of the calculated structure (red) on the X-ray structure (Molecule A – Black; Molecule B – blue) for compound (**1**).

Mulliken analysis

The atomic charge in molecules is fundamental to chemistry. For instance, atomic charge has been used to describe the processes of electronegativity equalization and charge transfer in chemical reactions[14,15] and to model the electrostatic potential outside molecular surfaces.[16-18] Mulliken atomic charges calculated at the B3LYP/6-311G(d,p) methods are collected in Table 4. It is worthy to mention that C19, C17, C15, C14, C13, C11 and C9 atoms of title compound exhibit positive charges, while other carbon atoms exhibit negative charges. Nitrogen N4 and N6 has a negative charge value. The charge values for Nitrogen N4, N6, Cl1 and C10 atoms are -0.4137, -0.4654, -0.0518 and -0.2498 a.u., respectively. The positive atomic charge is obtained for H10B and H6B is 0.1429 and 0.2228 a.u., respectively. However, all the hydrogen atoms exhibit a net positive charge. These magnitudes are changing between -0.4659 and 0.2228 a.u. The presence of large negative charge on Cl1, C10, N6 and N4 atoms and net positive charge on H10B and H6B atoms may confirms the formation of C10–H10B**…**N4 and N6–H6B**…**Cl1 intramolecular interactions in solid forms.

Table 4. Mulliken atomic charges of compound (**1**) at DFT level

Atoms	Atomic charges	Atoms	Atomic charges
Cl1	-0.0518	C15	0.0543
Cl2	-0.0593	C16	-0.2359
N1	-0.3279	C17	0.1421
N2	-0.0296	C18	-0.2372
N3	-0.2396	C19	0.0242
N4	-0.4137	C20	-0.0220
N5	-0.3862	H6A	0.2228
N6	-0.4654	H1	0.1126
C1	-0.0443	H6B	0.2248
C2	-0.0908	H2	0.1023
C3	-0.0846	H3	0.0998
C4	-0.0920	H4	0.0981
C5	-0.0712	H5	0.0875
C6	-0.1348	H7A	0.1275
C7	-0.0122	H7B	0.1606
C8	-0.0634	H10A	0.1381
C9	0.2801	H10B	0.1429
C10	-0.2498	H10C	0.1198
C11	0.1425	H12	0.1395
C12	-0.0465	H17	0.1405
C13	0.1208	H19	0.1209
C14	0.4470	H20	0.1094

Molecular orbital studies

The most widely used theory by chemists is the molecular orbital (MO) theory. The frontier molecular orbitals play an important role in the electronic and optical properties, as well as in UV-VIS spectra and chemical reactions.[19] The DFT calculated electronic absorption spectra, the maximum absorption wavelength corresponding to the electronic transition is from the highest occupied molecular orbital (HOMO) to the lowest unoccupied molecular orbital (LUMO). The frontier molecular orbital energies of the title compound are shown in Fig. 4.

The energy gap between HOMO and LUMO is a critical parameter in determining molecular electrical transport properties.[20,21] The lowest unoccupied molecular orbital (LUMO) energy is -1.7557 eV and the highest occupied molecular orbital (HOMO) energy is -6.2222 eV. The energy gap of HOMO–LUMO explains the ultimate charge transfer interaction within the molecule, and the frontier orbital energy gap of title compound is found to be -4.4665 eV obtained at DFT method using 6-311G(d,p) basis set. Lower the HOMO–LUMO gap explains the eventual charge transfer interactions taking place within the molecule, which influences the biological activity of the molecule.

Chemical reactivity

Chemical reactivity indices like chemical hardness (η), electronegativity (χ), electronic chemical potential (μ), and electrophilicity Index (ω), are calculated using DFT.

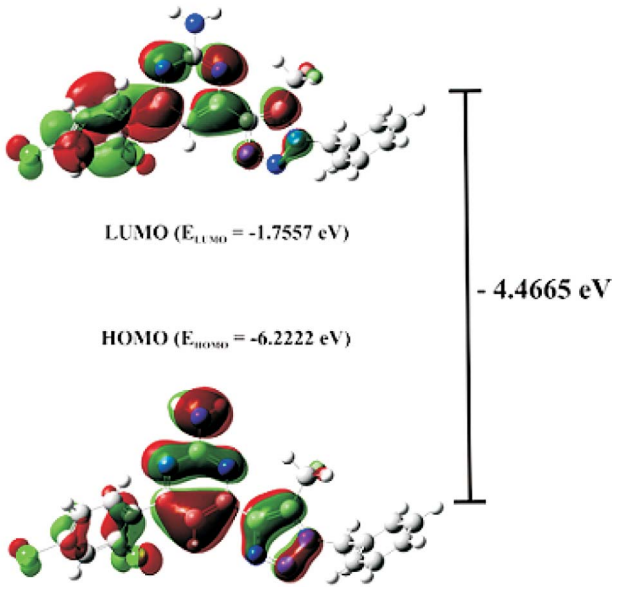

Fig. 4. The molecular orbital's and energies for the HOMO and LUMO of the title compound.

Chemical hardness is associated with the stability and reactivity of a chemical system. In a molecule, it measures the resistance to change in the electron distribution or charge transfer. On the basis of frontier molecular orbitals, chemical hardness corresponds to the gap between the Highest Occupied Molecular Orbital (HOMO) and Lowest Unoccupied Molecular Orbital (LUMO). Chemical hardness is approximated using equation $\eta = (E_{LUMO} - E_{HOMO})/2$, where E_{LUMO} and E_{HOMO} are the LUMO and HOMO energies, respectively. The larger the HOMO–LUMO energy gap, the molecule will be harder, more stable and less reactive. Table 5 (row 4) contains the computed chemical hardness value for title compound.

The concept of electronegativity put forward by Pauling[22] is defined as "the power of an atom in a molecule to attract electrons towards itself". Higher is the electronegativity of the species, greater is its electron accepting power or rather the electrophilicity. Electronegativity is determined using equation $\chi = -(E_{HOMO} + E_{LUMO})/2$, Table 5 (row 6) contains the computed electronegativity values for the title compound.

Electronic chemical potential is defined as the negative of electronegativity of a molecule[23] and determined using equation $\mu = (E_{HOMO} + E_{LUMO})/2$. Physically, μ describes the escaping tendency of electrons from an equilibrium system.[24] The value of μ for the title compound is presented in Table 5 (row 5).

Global electrophilicity index (ω), introduced by Parr, is calculated using the electronic chemical potential and chemical hardness as shown in equation $\omega = \mu^2/2\eta$. Electrophilicity index measures the propensity or capacity of a species to accept electrons.[25,26] It is a measure of the stabilization in energy after a system accepts additional amount of electronic charge from the environment.[27,28] The electrophilicity values of the title compound is presented in (Table 5, row 7).

Table 5. Calculated energy values of compound (**1**)

Basis set	B3LYP/6-311G(d, p)
E_{HOMO} (eV)	-6.222
E_{LUMO} (eV)	-1.756
E_{HOMO} - E_{LUMO} gap (eV)	-4.466
Chemical hardness (η)	2.233
Chemical potential (μ)	-3.989
Electronegativity (χ)	3.989
Electrophilicity index (ω)	3.563

The HOMO and LUMO orbital energies are related to gas phase ionization energies (I) and electron affinities (A) of the isomers according to the Koopmans' theorem through equations $A = -E_{LUMO}$, $I = -E_{HOMO}$. Electron affinity refers to the capability of a ligand to accept precisely one electron from a donor.

Molecular electrostatic potential

The molecular electrostatic potential (MEP) is a plot of electrostatic potential mapped onto the constant electron density surface. The MEP has been used primarily for predicting sites and relative reactivity towards electrophilic attack, in studies of biological recognition and hydrogen bonding interactions.[29,30] The negative electrostatic potential corresponds to an attraction of the proton by the concentrated electron density in the molecule (and is coloured in shades of red on the EPS surface), the positive electrostatic potential corresponds to repulsion of the proton by atomic nuclei in regions where low electron density exists and the nuclear charge is incompletely shielded (and is coloured in shades of blue). Potential increases in the order red < orange < yellow < green < blue.

Fig. 5 shows the molecular electrostatic potential (MEP), was determined using B3LYP/6-311G(d, p) method. The different values of the electrostatic potential at the surface are represented by different colours. As can be seen in Fig. 6, the negative (red) region is localized on the unprotonated atom of N5 and Cl1, with a minimum value of -0.034 and -0.0204 a.u., respectively. However, maximum positive (blue) region is localized on atom N6 and C19 probably due to hydrogen H6 and H19 with a value of 0.046 and 0.035 a.u., respectively and green represents region of zero potential. Therefore, Fig. 5 confirms the existence of an intermolecular N–H…N, N–H…Cl and C–H…Cl interactions.

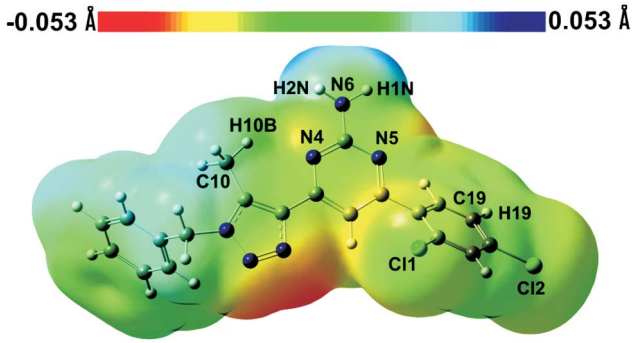

Fig. 5. Molecular electrostatic potential map calculated using B3LYP/6-311G(d, p) level.

Thermodynamic properties

The thermodynamics parameters of the compound have also been computed in order to get reliable relations among energetic, structural and reactivity characteristics of the molecules. Knowledge of permanent dipole moment of a molecule allows us to determine molecule's conforma-

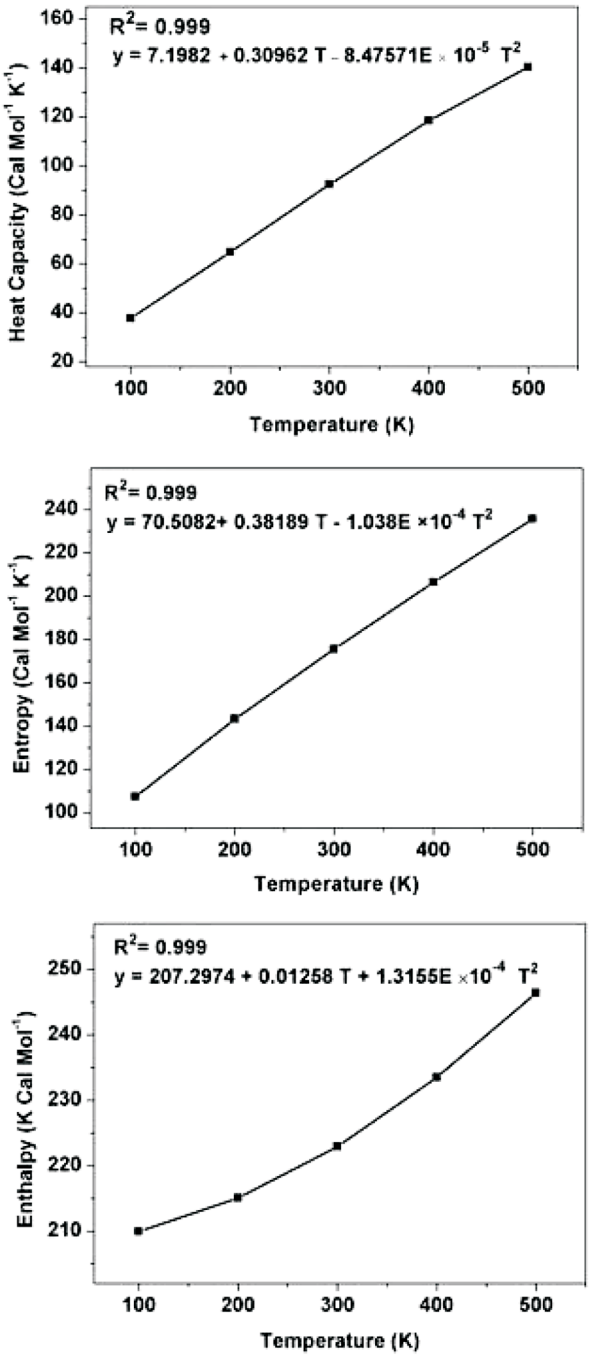

Fig. 6. Variation of thermodynamic parameters with temperature for compound (**1**).

tion. The values of thermodynamic parameters such as zero-point vibrational energy, thermal energy and dipole moment of title compound by Hartree-Fock(HF) and DFT methods with same 6-311G (d,p) basis set at 298.15 K and 1 atm pressure were calculated and listed in Table 6. From Table 6, the high value of dipole moment of title compound obtained by HF and DFT methods signifies high delocalization of charges, resulting in the formation of relatively loose structured and charge separated species.

The temperature dependence of the thermodynamic properties such as heat capacity at constant pressure ($C^{\circ}_{p,m}$), entropy (S°_{m}) and enthalpy (H°_{m}) for the title compound have been determined by B3LYP/6-311G(d,p) method in temperature range 100–500 K and listed in Table 7. From Table 7, it can be observed that these thermodynamic parameters increase with rise of temperature due to the fact that the molecular vibrational thermal energies increase with temperature. The correlation equations between heat capacities, entropies, enthalpy changes and temperatures were fitted by quadratic formulas given in equations. Below, and the corresponding fitting factors (R^2) for these thermodynamic properties were found to be 0.999. The temperature dependence correlation graphs are shown in Fig.7.

$$C^{\circ}_{p,m} = 7.1982 + 0.30962\ T - 8.47571\ E \times 10^{-5}\ T^2 \quad (R^2 = 0.9993)$$

$$S^{\circ}_{m} = 70.5082 + 0.38189\ T - 1.038E \times 10^{-4}\ T^2 \quad (R^2 = 0.9999)$$

$$H^{\circ}_{m} = 207.2974 + 0.01258\ T + 1.3155E \times 10^{-4}\ T^2 \quad (R^2 = 0.999)$$

Table 6. Thermodynamical parameters of compound (**1**) at 298K

Parameters	HF/6-311G(d, p)	B3LYP/6-311G(d, p)
Total energy (Hartree)	-2012.26	-2020.99
Zero point energy (K cal.mol^{-1})	222.706	207.568
Rotational constants (GHz)	0.34544	0.34189
	0.05590	0.05570
	0.05398	0.07176
Specific heat (C_v) (cal.mol^{-1}K^{-1})	85.500	91.961
Entropy (cal.mol^{-1}K^{-1})		
Total	169.735	174.975
Translational	43.925	43.925
Rotational	36.976	37.000
Vibrational	88.834	94.050
Dipole moment (Debye)	6.6392	6.6033

These equations could be used for further studies on the title compound. For instance, when the interaction of title compound with another compound is studied, these thermodynamic properties could be obtained from the above equation and then can be used to calculate the change in Gibbs free energy of the reaction, which will in turn help to judge the spontaneity of the reaction.

Interpretation of antibacterial activity

Each zone size is interpreted by reference to the Table 2G (Zone Diameter Interpretative Standards and equivalent Minimum Inhibitory Concentration Breakpoints) of the NCCLS M100-S12: Performance Standards for Antimicrobial Susceptibility Testing: Twelfth Informational Supplement.[31] Results indicated that target compound exhibited significant antimicrobial activity against selected pathogens, *Bacillus cerus*, *Escherichia coli*, *Acinetobacter baumann*, *Staphylococcus epidermidis* and *Proteus vulgaris* when compared with the standard antibiotic ciprofloxacin (25 μg).

The compound exhibits good antibacterial activity against Escherichia coli and Acinetobacter baumannii and exhibits moderate activity against Bacillus cereus, Staphylococcus epidermidis and Proteus vulgaris as shown in Table 8.

EXPERIMENTAL

Synthesis of (1): The title compound (**1**) was obtained according to the reaction Scheme 1.[32] A mixture of (E)-1-(1-benzyl-5-methyl-1H-1,2,3-triazol-4-yl)-3-(2,4-dichlorophenyl)prop-2-en-1-one(0.2 g, 0.53 mmol), guanidine hydrochloride (0.15 g, 1.57 mmol) and NaOH (0.04 g, 1.0 mmol) in ethanol (10 mL) was refluxed for 40 min. Then, the reaction mixture was poured onto excess crushed ice and neutralized with dilute hydrochloric acid. The precipitated 4-(1-benzyl-5-methyl-1H-1,2,3-triazol-4-yl)-6-(2,4-dichlorophenyl)pyrimidin-2-amine was filtered and recrystallized from ethanol. Needle like colourless single crystals of the title compound used in X-ray diffraction studies were grown

Table 7. Thermodynamic properties at different temperatures of compound (**1**) at B3LYP/6-311G(d, p) level

Temperature (K)	$C^{o}_{p,m}$ (cal.mol^{-1}K^{-1})	S^{o}_{m} (cal.mol^{-1}K^{-1})	H^{o}_{m} (Kcal.mol^{-1})
100	37.800	107.427	209.900
200	64.755	143.259	215.025
300	92.469	175.558	222.886
400	118.449	206.369	233.460
500	140.338	235.679	246.437

Table 8. Antibacterial activity of compound (**1**) at different concentrations against bacterial pathogens

Microorganisms	Zone of inhibition (mm)			
	Compound concentration			Positive control
	(25 μg/ml)	(50 μg/ml)	(75 μg/ml)	CIPX (25 μg)
Bacillus cereus (MTCC 430)	24	30	36	38
Staphylococcus epidermidis (MTCC 10623)	18	20	23	24
Escherichia coli (MTCC 443)	30	36	42	30
Acinetobacter baumannii (MTCC 1425)	21	24	28	18
Proteus vulgaris (MTCC 742)	18	21	27	30

in an ethanolic solution by slow evaporation of the solvent at room temperature and collected in 79% yield.

Scheme 1 Reaction scheme and chemical diagram of the title compound (**1**)

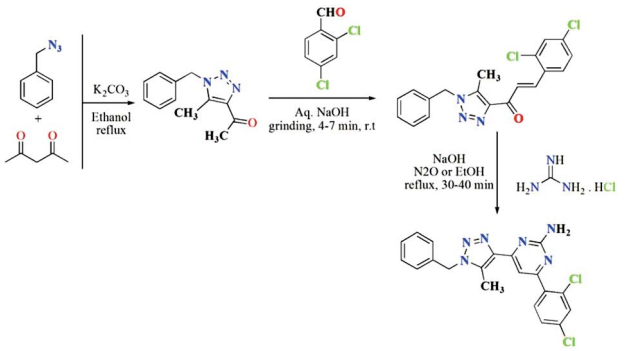

White solid; m.p. 181 °C, Yield: 79%. **^{1}H NMR (300 MHz, CDCl3):** δ 7.80 (1H, s, =CH), 7.56-7.50 (2H, m, ArH), 7.35-7.33 (4H, m, ArH), 7.26 (1H, s, ArH), 7.26-7.20 (1H, m, ArH), 5.56 (2H, s, C_6H_5-CH_2), 5.14 (2H, brs, NH_2), 2.62 (3H, s, CH3); **^{13}C NMR (75 MHz, CDCl3):** δ 165.67, 163.15, 160.10, 139.05, 134.56, 134.02, 129.68, 129.11, 129.06, 128.40, 127.19, 119.74, 116.82, 112.09, 104.60, 51.62, 9.73.

X-ray Crystallography: The Crystal of the title compound having approximate dimension 0.30 × 0.24 × 0.11 mm^3 was mounted on a glass fiber using cyanoacrylate adhesive. All measurement were made on a Bruker AXS Kapppa Apex II single crystal X-ray diffractometer using graphite mono-chromated MoKα (λ = 0.71071 Å) radiation and CCD detector. Diffraction data were collected at room temperature by the ω-scan technique. Accurate unit cell parameters and orientation matrix were obtained by a least-squares fit of several high angle reflections in the ranges 1.90° < θ < 28.36° for the title compound. The unit cell parameters were determined for 36 frames measured (0.5° phi-scan) from three different crystallographic zones and using the method of difference vectors. The intensity data were collected with an average four-fold redundancy per reflection and optimum resolution (0.75 Å). The intensity data collection, frames integration, Lorentz-polarization correction and decay correction were done using SAINT-NT (version 7.06a) software. Empirical absorption correction (multi-scan) was performed using SADABS[33] program. The structure was solved by direct methods using SHELXS-97 implemented in WinGX[34] program suit. The refinement was carried out by full-matrix least-square method on the positional and anisotropic temperature parameters of the non-hydrogen atoms, using SHELXL-97.[35] All the H atoms were positioned geometrically and constrained to ride on their parent atom with C–H = 0.93–0.97 Å and N–H = 0.86 Å, and with U_{iso}(H) = 1.5 U_{eq} for methyl H atoms and 1.2 U_{eq}(C) for other H atoms. Owing to poor agreement, the reflection [1 1 0], was omitted from the final cycles of refinement. The general-purpose crystallography tool PLATON,[36] ORTEP[37] and MERCURY[38] were used for structure analysis and presentation of the results. Crystallograhic data for the structure reported in this article have been deposited in the Cambridge Crystallographic Data Center with a supplementary publication number of CCDC 1001329. Copies of these information can be obtained free of charge from the Director, CCDC, 12 Union Road, Cambridge CB2 1EZ, UK (fax: +44 1223 336 033; e-mail: deposit@ccdc.cam.ac.uk).

Computational details: The molecular structure of the compound in ground state (in vacuo) was optimized using density functional theory DFT (B3LYP)[39,40] method with the 6-311G(d,p)[41] basis set. All the calculation was performed without specifying any symmetry for the title molecule by using GaussView molecular visualization program[42] and Gaussian 03 program package.[43] The optimized geometrical parameters, energy, atomic charges and dipole moments were calculated using Gaussian 03W package. GaussView 03 program has been using to construct optimized molecular geometry, Mullikan charges, HOMO-LUMO energy gap,[44,45] Molecular electrostatic potential, chemical reactivity and thermodynamic properties.

Antibacterial test: Antibacterial susceptibility test was carried out using Kirby-bauer disk diffusion method as per CLSI M38-A guidelines.[46]

The synthesized compound was dissolved in DMSO at various concentrations (25, 50 and 75 μg/ml) and tested against selected bacterial pathogens. Suspension of bacterial isolates was adjusted to 0.5 McFarland standards in 0.85% saline (suspension

will contain approximately 4×10^8 CFU/ml) and lawn culture was spread using sterile swabs on Muller Hinton agar media (Hi-media, Mumbai). Wells (6 mm/dm, 2 cm apart) were bored upon the lawn culture of the agar media using a sterile borer. Test compound (25, 50 and 75 μg/ml) were loaded to the wells under aseptic conditions and the plates were incubated at 37 °C for 24 hours. Presence of inhibition zones surrounding each well evidenced antimicrobial activity. The antimicrobial activity was evaluated by measuring the inhibition zones diameter in millimeters. Each experiment was repeated three times and the mean of inhibitory zones were recorded. Tests strains were procured from MTCC, INTECH, Chandigarh, India. They include *Bacillus cerus* (MTCC 430), *Escherichia coli* (MTCC 443), *Acinetobacter baumannii* (MTCC 1425), *Staphylococcus epidermidis* (MTCC 10623), and *Proteus vulgaris* (MTCC 742). Standard antibiotic ciprofloxacin (25 μg) was used as positive control to perform the test.

CONCLUSIONS

The title compound was synthesized and has been confirmed by NMR and structural (single-crystal X-ray diffraction) techniques. To support the solid state structure, the geometric parameters of the title compound have been calculated using density functional theory DFT (B3LYP) method with the 6-311G(d,p) basis sets, and compared with the experimental findings. It was noted here that the experimental results belong to solid phase and theoretical calculations belong to gaseous phase. In the solid state, the existence of the crystal field along with the intermolecular interactions have connected the molecules together, which result in the differences of bond parameters between the calculated and experimental values. The small HOMO-LUMO gap value shows that the molecule is biologically active. The MEP map shows that the negative potential sites are on nitrogen and chlorine atoms as well as the positive potential sites are around the hydrogen atoms and hence MEP map confirms the existence of intermolecular N–H**…**N, C–H**…**Cl and N–H**…**Cl interactions. The calculated HOMO and LUMO energies can be used to semi quantitatively estimate the ionization potential, electron affinity, electronegativity, electrophilicity index, hardness, and chemical potential. The correlations between the statistical thermodynamics and temperature are also obtained. It is seen that the heat capacities, entropies and enthalpies increase with the increasing temperature owing to the intensities of the molecular vibrations increase with increasing temperature. The obtained antibacterial activity results indicate that the compound exhibit good to moderate activity against tested pathogens.

ACKNOWLEDGEMENTS

The authors thank Dr. Shibu M. Eapen, STIC, Cochin, India, for his help with the data collection.

REFERENCES

1. Morales-Sanfrutos, J.; Ortega-Munoz, M.; Lopez-Jaramillo, J.; Hernandez-Mateo, F.; Santoyo-Gonzalez, F. *J. Org. Chem.* **2008**, *73*, 7768-7771.
2. Genin, M. J.; Allwine, D. A.; Anderson, D. J.; Barbachyn, M. R.; Emmert, D. E.; Garmon, S. A.; Graber, D. R.; Grega, K. C.; Hester, J. B.; Hutchinson, D. K.; Morris, J.; Reischer, R. J.; Ford, C. W.; Zurenko, G. E.; Hamel, J. C.; Schaadt, R. D.; Stapert, D.; Yagi, B. H. *J. Med. Chem*. **2000**, *43*, 953-970.
3. Buckle, D. R.; Rockell, C. J. M.; Smith, H.; Spicer, B. A. *J. Med. Chem.* **1986**, *29*, 2262-2267.
4. Giffin, M. J.; Heaslet, H.; Brik, A.; Lin, Y. C.; Cauvi, G.; Wong, C. H.; McRee, D. E.; Elder, J. H.; Stout, C. D.; Torbett, B. E. *J. Med. Chem.* **2008**, *51*, 6263-6270.
5. Wang, S.; Wang, Q.; Wang, Y.; Liu, L.; Weng, X.; Zhang, G. L. X.; Zhou, X. *Bioorg. Med. Chem. Lett.* **2008**, *18*, 6505-6508.
6. El-Subbagh, H. I.; Abu-Zaid, S. M.; Mahran, M. A.; Badria, F. A.; Al-Obaid, A. M. *J. Med. Chem.* **2000**, *43*, 2915-2921.
7. Trivedi, A. R.; Dodiya, D. K.; Ravat, N. R.; Shah, V. H. *Arkivoc* **2000**, *XI*, 131-141.
8. Koch, W.; Holthausen, M. C. A. *A Chemistry Guide to Density Functional Theory*; Wiley-VCH: Weinheim, New York, Chichester, 2000
9. Parr, R. G.; Yang, W. T. *Density Functional Theory of Atoms and Molecules*; Oxford University Press: New York, 1989.
10. Huang, C.-C.; Wu, F.-L.; Lo, Y. H.; Lai, W.-R.; Lin, C.-H. *Acta. Cryst.* **2010**, *E66*, o1690.
11. Sarmiento-Sánchez, J. I.; Aguirre, G.; Rivero, I. A. *Acta Cryst.* **2011**, *E67*, o1856.
12. Bukhari, M. H.; Siddiqui, H. L.; Chaudhary, M. A.; Hussaina, T.; Parvezc, M. *Acta Cryst.* **2008**, *E64*, o963.
13. Jian, F. F.; Zhao, P. S.; Bai, Z. S.; Zhang, L. *Struct. Chem.* **2005**, *16*, 635-639.
14. Jug, K.; Maksic, Z. B. *Theoretical Model of Chemical Bonding*; Springer: Berlin, 1991.
15. Fliszar, S. *Charge Distributions and Chemical Effects*; Springer: Berlin, Heidelberg, New York, 1933.
16. Smith, P. E.; Montgomery Pettitt, B. *J. Am. Chem. Soc.* **1991**, *113*, 6029-6037.
17. Gao, J. *J. Chem. Phys*. **1993**, *98*, 1975-1981.
18. Cieplak, P.; Kollman, P. *J. Comput. Chem.* **1991**, *12*, 1232-1236.
19. Fleming, I. *Frontier Orbitals and Organic Chemical Reactions*; Wiley: London, 1976.

20. Fukui, K. *Science* **1982**, *218*, 747-754.
21. Udhayakala, P.; Rajendiran, T. V.; Seshadri, S.; Gunasekaran, S. *J. Chem. Pharm. Res.* **2011**, *3*(3), 610-625.
22. Pauling, L. *The Nature of Chemical Bond*; Cornell University Press: Ithaca, 1960.
23. Parr, R. G.; Pearson, R. G. *J. Am. Chem. Soc.* **1983**, *105*, 7512.
24. Chattaraj, P. K.; Maiti, B. *J. Am. Chem. Soc.* **2003**, *125*, 2705.
25. Vektariene, A.; Vektaris, G.; Svoboda, J. *ARKIVOC* **2009**, *7*, 311.
26. Parr, R. G.; Szentpaly, L.; Liu, S. *J. Am. Chem. Soc.* **1999**, *121*, 1922.
27. Koopmans, T. *Physica* **1933**, *1*, 104.
28. Liu, S. *J. Chem. Sci.* **2005**, *117*, 477.
29. Murray, J. S.; Sen, K. *Molecular Electrostatic Potentials, Concepts and Applications*; Elsevier: Amsterdam, 1996; pp 7-624.
30. Scrocco, E.; Tomasi, J. *Adv. Quant. Chem.* **1978**, *11*, 115.
31. National Committee for Clinical Laboratory Standards (NCCLS). Performance Standards for Antimicrobial Susceptibility Testing; 2002 Twelfth Informational Supplement, Wayne, PA, M100-S.
32. Nagarajan, S.; Shanmugavelan, P.; Sathishkumar, M.; Selvi, R.; Ponnuswamy, A.; Harikrishnan, H.; Shanmugaiah, V. *Chin. Chem. Lett.* **2014**, *25*, 419-422.
33. Bruker, APEX-II, SAINT-Plus (Version 7.06a), (BrukerAXS Inc. Madion, Wisconsin, USA, 2004).
34. Farrugia, L. J. *J. Appl. Cryst.* **1999**, *32*, 837.
35. Sheldrick, G. M. *Acta Cryst.* **2008**, *A64*, 12.
36. Spek, A. L. *J. Appl. Cryst.* **2003**, *36*, 7.
37. Farrugia, L. J. *J. Appl. Cryst.* **1997**, *30*, 565.
38. Bruno, I. J.; Cole, J. C.; Edgington, P. R.; Kessler, M.; Macrae, C. F.; McCabe, P.; Pearson, J.; Taylor, R. *Acta Cryst.* **2002**, *B58*, 389.
39. Becke, A. D. *J. Chem. Phys*. **1993**, *98*, 648.
40. Lee, C.; Yang, W.; Parr, R. G. *Phys. Rev.* **1998**, B37, 785.
41. Ditchfield, R.; Hehre, W. J.; Pople, J. A. *J. Chem. Phys.* **1971**, *54*, 724-728.
42. Dennington, II., R.; Keith, T.; Millam, J. *GaussView (Version 4.1.2.)* Semichem Inc.: Shawnee Mission, 2007.
43. Frisch, M. J.; Trucks, G. W.; Schlegel, H. B.; Scuseria, G. E.; Robb, M. A.; Cheeseman, J. R.; Montgomery, Jr., J. A.; Vreven, T.; Kudin, K. N.; Burant, J. C.; Millam, J. M.; Iyengar, S. S.; Tomasi, J.; Barone, V.; Mennucci, B.; Cossi, M.; Scalmani, G.; Rega, N.; Petersson, G. A.; Nakatsuji, H.; Hada, M.; Ehara, M.; Toyota, K.; Fukuda, R.; Hasegawa, J.; Ishida, M.; Nakajima, T.; Honda, Y.; Kitao, O.; Nakai, H.; Klene, M.; Li, X.; Knox, J. E.; Hratchian, H. P.; Cross, J. B.; Adamo, C.; Jaramillo, J.; Gomperts, R.; Stratmann, R. E.; Yazyev, O.; Austin, A. J.; Cammi, R.; Pomelli, C.; Ochterski, J. W.; Ayala, P. Y.; Morokuma, K.; Voth, G. A.; Salvador, P.; Dannenberg, J. J.; Zakrzewski, V. G.; Dapprich, S.; Daniels, A. D.; Strain, M. C.; Farkas, O.; Malick, D. K.; Rabuck, A. D.; Raghavachari, K.; Foresman, J. B.; Ortiz, J. V.; Cui, Q.; Baboul, A. G. Clifford, S.; Cioslowski, J.; Stefanov, B. B.; Liu, G.; Liashenko, A.; Piskorz, P.; Komaromi, I.; Martin, R. L.; Fox, D. J.; Keith, T.; Al-Laham, M. A.; Peng, C. Y.; Nanayakkara, A.; Challacombe, M.; Gill, P. M. W.; Johnson, B.; Chen, W.; Wong, M. W.; Gonzalez, C.; Pople, J. A. Gaussian 03, Revision B.05. 2004 Gaussian Inc.: Pittsburgh.
44. Frisch, A. E.; Nielsen, A. B.; Holder, A. J. *Gaussview* Gaussian Inc.: Pittsburgh, 2003.
45. Young, D. C. *Computational Chemistry: A Practical Guide for Applying Techniques to Real-World Problems*; John Wiley & Sons Inc.: New York, 2001.
46. Bauer, A. W.; Kirby, W. M. M.; Sherris, J. C.; Turck, M. *Am. J. Clin. Pathol.* **1966**, *45*, 493.

